

# A Novel Scheme on Fault Diagnosis of Induction Motors using Current per Voltage Bode Diagram

Widagdo Purbowaskito\*\*, Chen-Yang Lan\*, Meng-Kun Liu\* and Kenny Fuh\*\*\*

**Keywords:** bode diagram, fault detection and diagnosis, frequency-domain, induction motor, MCSA

## ABSTRACT

Unexpected failure of industrial motors is costly in production loss and is time consuming in repairing process. Motor current signature analysis has been used for fault diagnosis and detection but this method is depended on the voltage input quality and motor loading level in order to achieve accurate results. In this study, a novel motor fault detection and diagnosis method is proposed. The method is a preliminary study of a new approach in model-based fault detection and diagnosis method. It works by analyzing the bode diagram of the induction motor that will be generated by using current per voltage ratio in frequency-domain. Five industrial induction motors with three different conditions are the examples in this study. Two induction motors are in healthy condition, two induction motors are operated under misalignment/unbalance fault, and one induction motor is operated under bearing fault condition. The study results show that the proposed bode diagram approach can be used to detect the motor faults and the difference patterns appeared are visibly notable for the fault detection and diagnosis (FDD) of motor condition.

*Paper Received June, 2020. Revised September, 2020. Accepted November, 2020. Author for Correspondence: Chen-Yang Lan.*

*\* Assistant Professor, Department of Mechanical Engineering, National Taiwan University of Science and Technology, Taipei, Taiwan 106, R.O.C.*

*\*\* PhD Student, Department of Mechanical Engineering, National Taiwan University of Science and Technology, Taipei, Taiwan 106, R.O.C.*

*\*\*\* Engineering Division, Innolux Corporation, Jhunan Science Park, Miaoli County, 35053, R.O.C.*

## INTRODUCTION

Induction motors have been used to power board range of applications in industry. But often, motors run not in their proper condition which reduce its production efficiency and increase cost in energy consumption. While sudden failures and malfunction of these motors lead to discontinuity of production which mostly results in time consuming and expensive repairing process. In this era of industry 4.0, condition monitoring of induction motors has drawn significant consideration in building of motor health management system in order to improve the reliability and safety of the production system. In the past, a safe and reliable operation of motor is ensured by performing simple detections of overcurrent, overvoltage and earth-fault (Nandi, Toliyat and Li, 2005). These traditional techniques are unable to locate the specific failure features or provide classification information that leads directly to the root cause of the motor failures (Wang *et al.*, 2019). As the operation of the motor becoming more complex, these simple detection techniques are not enough. Especially in the condition of which the unexpected motor shut down is not tolerated.

In general, motor failures can be classified as bearing failures, stator winding failures, broken rotor bars, air gap eccentricity, and other failures (Thomson and Culbert, 2017). As in the induction motor operation, bearing failures, stator short turn, broken rotor bar, misalignment, and air gap eccentricity are among the most common ones and thus require special attention and treatment. These failures generally bring one or more symptoms such as, air gap voltage and line current unbalance, high pulsations of torque, decline of average torque output, low in efficiency, and excessive increase in temperature (Nandi, Toliyat and Li, 2005). Early detection of these failure symptoms of the induction motor helps us to avoid the unexpected breakdown during the motor operation, and helps the motor to run in the proper condition with better energy efficiency. According to Sullivan *et al.*, (2010), efficiently operated

induction motor can reduce the energy consumption up to 5 – 20 %.

Currently, fault detection and diagnosis (FDD) are consisted of two major approaches such as, motor vibration spectrum analysis (MVSA) and motor current spectrum analysis (MCSA). Both can be analyzed through frequency-domain and time-frequency spectrum analyses. As the behavior of rotational machinery that react to internal or external forces, vibration can be used as the indication about the current condition of a rotational machinery. Excessive vibrations above the acceptable vibration limit (ISO 10816-3, 1998) can be an indicator that there are mechanical issues on the rotational machinery. ISO 10816-3, (1998) is a basic document describing a general criteria to analyze the vibration of various type of motor size, ranged from small to large motor sizes. A time-frequency spectrum analysis has proven that the vibration signal is a proper mechanical fault signature such as bearing faults (Liu and Weng, 2019).

Current spectrum can be used to observe the condition of the motor. It reflects the air-gap relationship between the stator and the rotor of the motor. Mostly, the presence of the faults will affect this relationship between the stator and the rotor in which can be observed from the stator current signal. If electrical or mechanical faults present on the motor, the current spectrum could be used to show that the faults are present. However, the current spectrum is not free from noises. Because noises may present due to the input voltage, and this causes the MCSA getting more difficult to be interpreted. Several methods have been developed in order to enhance the capability of MCSA based FDD. A detection of mechanical looseness of sleeve bearing is developed by only using the stator current spectrum (Jung *et al.*, 2016). As noises may present in the current spectrum, the detection of mechanical faults such as bearing faults in frequency-domain spectrum analysis is obscure. A time-frequency spectrum analysis is developed in order to overcome this such of limitation in detecting the fault signatures (Guo and Liu, 2018). Some characteristic frequencies identification related to mechanical and electrical faults rely on the accuracy of slip calculation. Thus, it may fail to detect the presence of the faults due to the inaccurate slip calculation. Another obstacle is the requirements of the detail of bearing type, model, and brand to calculate the characteristic frequencies of bearing faults. Without correct information, a slip calculation may be inaccurate. An MCSA based FDD is developed with optimal slip estimation to improve the accuracy of faults detection that requires the slip calculation (Jung, Lee and Kwon, 2006).

A combination of MCSA and MVSA approaches may have been sought to improve the accuracy of FDD. Popaleny and Antonino-Daviu (2018) combined the

MCSA and MVSA to improve the detection of these faults such as misalignment/unbalance, looseness, broken rotor bars and bearing faults. However, it is possible only to do that in a controlled laboratory environment. Industrial factories in fact are highly disturbing environment especially for vibration signal. One machine vibration signal may be affected by other machines' vibration. The requirement of correct vibration sensor location for specific fault signal also makes it difficult to collect the exact vibration signal that represent some specific faults. For example, a non-drive end bearing faults detection require sensors to be located at non-drive end of the motor. Hence, it requires numbers of accelerometer transducers only for gathering the vibration signals for many specific faults detection. Therefore, this configuration will be costly only for one motor. In addition, the location or the configuration of the motor may not be accessible to place such of accelerometer transducer (Jung *et al.*, 2016). Especially in some location where the sensor or transducer are exposed to extreme environment such as nuclear plant, this will reduce the time span of sensor and require the sensor to be replaced periodically. This in fact brings the MVSA difficult to be applied in such industrial factories despite that its fact that vibration signal is sensitive for finding the mechanical faults with the correct sensor location.

In opposite of MVSA limitations, MCSA has advantages in collecting the current signals. MCSA needs only one phase of current data for analysis, while in many motors the current sensors have already installed during the motor installation in the factory. The source of noises that may present in the current signals come mostly from the voltage supply source. However, current spectrum magnitude is depended on the motor loading level. If the loading level is low, then the current spectrum magnitude is also low. Hence, this will also affect the fault frequency magnitude. The lower the load level the lower the fault frequency magnitude, and with a noisy spectrum, the identification of fault frequency in low loading level getting more difficult. Generally, the MCSA based FDD consider only for one phase of current signal to be analyzed which in fact requires good voltage supply and high loading level for the successfulness of faults detection. However, industrial factories may have inefficient loading and highly disturbing voltage source which makes the MCSA more challenging.

In this study, a novel method of motor current per voltage bode diagram based analysis is proposed. This proposed method will consider the voltage input and the current output of the induction motor. Hence, it can be said that this method will be a preliminary and lower cost approach in model-based FDD. An assumption is made that the system is a linear time invariant system in a

quasi-steady state condition. A quasi-steady state is a condition in which a system is assumed to be in steady state condition but a small perturbation or small transient is allowed to be appear in the system output. Therefore, in this study a 6 seconds 3-phase voltage and current are acquired when the motor has passed the initial transient condition and run in stable operation frequency. By this assumption, it is expected that a particular solution of the system as a linear time invariant system can be drawn. At certain frequency a linear time invariant induction motor model will generate a bode diagram at certain magnitude and phase. Because bode diagram represents the relationship between the linear system model input and output, the system condition can be observed through this relationship. The proposed methodology works by finding the specific harmonics of motor in frequency spectrum of current per voltage waveform. Besides these harmonics, the presence of fault and other significant peaks frequencies will also be identified. The results of harmonics, fault, and significant peak frequencies identification will be plotted in logarithmic magnitude and phase plots. These plots will be employed to identify the presence of the faults.

In this paper, five sections are presented. First section is this section of introduction. The second section present the motor fault characteristic frequency identification. The third section presents the methodology proposed in this study. The fourth section presents the results and discussions. While the fifth section presents the conclusions, recommendations drawn from this study, and the future work.

## IDENTIFICATION OF MOTOR FAULTS AND ITS CHARACTERISTIC FREQUENCY SPECTRUMS

ISO 20958 (2013) provides the standard of induction motor online condition monitoring and standard in finding the motor fault characteristic frequencies in motor current. Different fault characteristic frequencies are found in ISO 20958 and can be calculated by following its guidelines.

### Bearing Faults

Defects on the bearing ball or rolling element will increase vibrations and noise level at each component rotational speed. About 40 – 50 % motor failures are related to bearing faults due to the internal operating stresses, and external issues such as poor lubrication, corrosion, contamination, and improper installation (Nandi, Toliyat and Li, 2005). These vibrations appear as characteristic frequencies in the frequency-domain spectrum. The characteristic frequencies are related to the bearing balls, inner and outer bearing raceways

defects. As bearing supports the rotor position at motor non-drive end and drive end by providing balance in air gap between rotor and stator, the condition of the bearing can be determined from these characteristic frequencies which provide a relationship to the stator current spectrum (Schoen *et al.*, 1995).

Defected bearing will generate a radial motion between rotor and stator. This radial motion results in mechanical displacement when the rotor rotating and causes the air gap between rotor and stator varying. The variations of the air gap cause the air gap flux density to vary and induce the stator voltage resulting in the stator current to contain bearing fault characteristic frequencies (Schoen *et al.*, 1995). The bearing fault characteristic frequencies in the current spectrum can be calculated by using Eq. (1) as follows,

$$f_{bearing} = |f_e \pm m f_v| \quad (1)$$

where  $m = 1, 2, 3, \dots$  and  $f_v$  is one of the bearing fault characteristic frequencies related to the bearing balls, inner and outer bearing raceways defects. These bearing fault characteristic frequencies can be calculated by using Eq. (2) to (4) as follows (Schoen *et al.*, 1995)(Jung, Lee and Kwon, 2006) (Guo and Liu, 2018),

$$f_{in} = f_e + \frac{N_B}{2} f_{shaft} \left( 1 + \frac{D_P}{D_B} \cos \alpha \right) \quad (2)$$

$$f_{out} = f_e + \frac{N_B}{2} f_{shaft} \left( 1 - \frac{D_P}{D_B} \cos \alpha \right) \quad (3)$$

$$f_{ball} = f_e + \frac{D_P}{D_B} f_{shaft} \left( 1 - \left( \frac{D_P}{D_B} \cos \alpha \right)^2 \right) \quad (4)$$

where  $f_{in}$ ,  $f_{out}$ , and  $f_{ball}$  are bearing fault characteristic frequencies related to inner bearing raceways, outer bearing raceways and bearing balls defects respectively,  $f_e$  is the supply frequency,  $f_{shaft}$  is the motor shaft rotational frequency,  $N_B$  is number of ball bearings,  $D_P$  is the pitch diameter,  $D_B$  is the ball bearing diameter, and  $\alpha$  is the bearing contact angle.

### Shaft Misalignment/Unbalance

Misalignment across the coupled motor shaft and the driven load causes an external pre-load force transmitted into the rotor. As the misalignment is higher, the transmitted pre-load force on the shaft and rotor getting higher, and pushing the shaft and the rotor to the side (Ortiz *et al.*, 2019). Several factors that generate a misalignment are such as, bend in rotor shaft, mechanical resonance at critical speed, and bearing looseness (Nandi *et al.*, 2010). Misalignment is one of the sources of motor dynamic eccentricity, while the static eccentricity is caused by either bearing faults and broken rotor bar. Static eccentricity appears when the rotor position is asymmetric and when the rotor is not installed properly.

Dynamic eccentricity is a condition where the rotor center is not located in the center of rotation and the smallest air-gap position rotates with the rotor (Nandi, Toliyat and Li, 2005). Therefore, air-gap in dynamic eccentricity is affected by the stator angle as the smallest air-gap position is rotated the rotor as the rotor rotates (Jung, Lee and Kwon, 2006). However, both static and dynamic eccentricity are likely to be found in induction motor during harsh or heavy duty cycle operation. For example, a static eccentricity due to broken rotor bar or bearing fault is not fixed properly. This eventually makes the static eccentricity getting more severe. In a case of severe static eccentricity, a high level of unbalanced magnetic pull (UMP) might be produced during a rotor rotation. This UMP generates misalignment and unbalance faults in motor shaft and rotor, and eventually leads to dynamic eccentricity (Nandi *et al.*, 2010).

When mix of both static and dynamic eccentricities appears during the motor operation, the variations of rotor position and oscillation in the radial air gap length will induce variations of air-gap flux density to the stator current. Therefore, two symmetrical sidebands may appear as the misalignment/unbalance characteristic fault frequency around the motor fundamental frequency given in Eq. (5) and (6) as follows (ISO 20958, 2013),

$$f_{miss} = f_e \pm m f_r \quad (5)$$

$$f_r = \frac{(1-s)}{p} f_e \quad (6)$$

where,  $f_{miss}$  is the misalignment/unbalance characteristic frequency,  $f_r$  is the rotational speed frequency of the rotor,  $P$  is the number of pole pairs and  $s$  is the slip.

## METHODOLOGY

### Experimental Setup and Data Collection Method

Three CT current sensors and three voltage sensors are used to collect the 3-phase current and voltage data of the induction motors. A data acquisition device with 2.5 kHz sampling rate is used. Fig 1. shows the configuration of current and voltage sensors during the data acquisition process. 3-phase current and voltage data is collected synchronously from the primary side of the induction motors. The length of the data collected for the analysis is 6 seconds length of time. The data collection is performed when the induction motor operating at steady state condition at certain rated frequency with fixed loading condition depended on what operation is the motor addressed. This provides steady state current and voltage data for further analysis.

### Fast Fourier Transform

Frequency-domain spectrum provides rich information regarding to a signal's unique frequency characteristic compare to time-domain signature. These unique frequency characteristics can be extracted from the signal to understand the motor condition during the operation. Fast Fourier transform (FFT) converts the motor current time-domain waveform into current frequency-domain spectrum with different frequency components. These components consist of harmonics and peaks that present in the motor signal during operation. These harmonics and peaks appeared in the current spectrum may due to the motor inverter frequency and its harmonics, or generated by different electrical and mechanical faults (Yang *et al.*, 2016).

FFT algorithm is used to compute this following Discrete Fourier Transform (DFT) presented in Eq. (7) as follows (Mitra and Kuo, 2006)(Hsu *et al.*, 2019),

$$X[k] = \sum_{n=0}^{N-1} x[n] e^{-j\frac{2\pi}{N}kn} \quad (7)$$

$$X[k] = \sum_{n=0}^{N-1} x[n] [\cos(\frac{2\pi}{N}kn) - j \sin(\frac{2\pi}{N}kn)] \quad (8)$$

where  $k = 0, 1, 2, 3, \dots, N - 1$ , and  $N$  is length of data.

### Motor Current Signature Analysis

By using Eq. (7) a time-domain current waveform is converted into a frequency-domain spectrum. This frequency-domain spectrum provides us information regarding to the presence of multiple frequency peaks in the current waveform, which are related to the motor condition. MCSA requires prior knowledge related to the motor operation condition such as operation frequency and motor rated RPM. In order to identify the fault frequencies, a knowledge regarding to some parts specification is also essential such as bearing geometry. The MCSA flowchart diagram is shown in Fig 2..

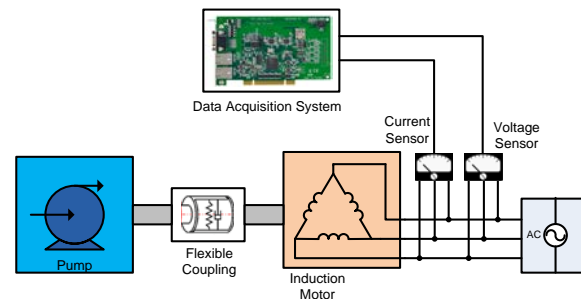


Fig. 1. 3-phase current and voltage data collection setup

### Motor Current per Voltage Bode Diagram Analysis

In this study, the proposed current per voltage bode diagram analysis works by considering all the important frequencies magnitude and phase of the system in current per voltage frequency spectrum. These important frequencies consist of motor harmonics which is considered up to 13<sup>th</sup> harmonics, fault frequencies that

may appear based on the Eq. (1) to (6), and any significant peak on the frequency-domain spectrum. The frequency band is limited up to 13th harmonics for the analysis due to the fault frequencies considered.

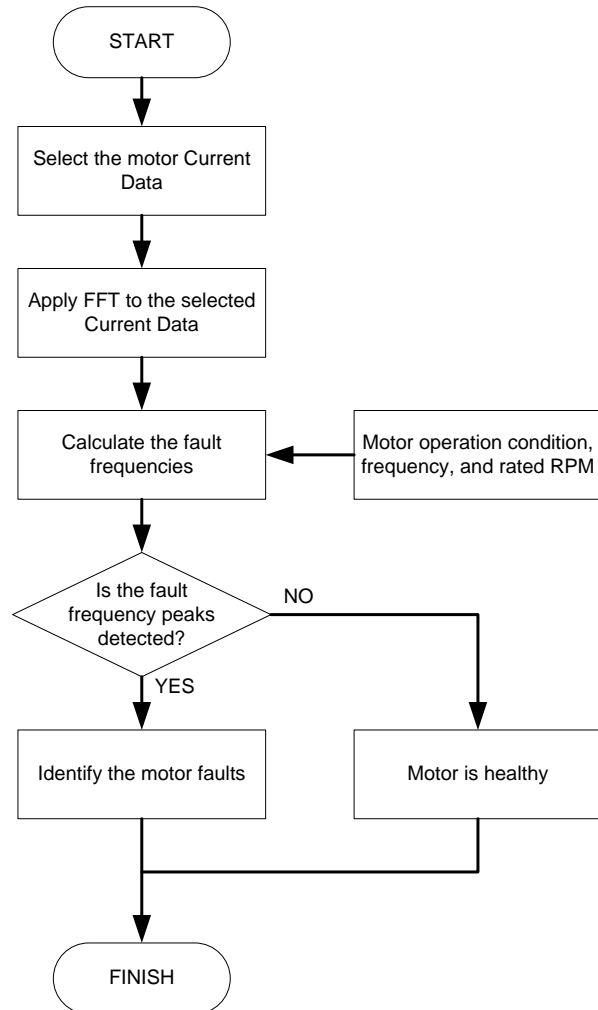


Fig. 2. Motor current signature analysis flowchart diagram

Fig. 3 shows the flowchart of current per voltage bode diagram analysis. Similar to MCSA, a prior information regarding to the motor operation condition, frequency, and rated RPM is needed. Motor operation frequency is needed to calculate the system harmonics, while operation condition, and rated RPM can be used to calculate the considered fault frequencies using Eq. (1) to (6) for misalignment/unbalance and bearing faults. Significant peak will not be calculated but its indexes will be identified together with harmonics and fault frequencies indexes during the windowing process for finding the indexes. The significant peaks are defined based on its magnitudes that higher than noise magnitudes.

Both current and voltage will be converted from time-domain waveform into frequency-domain spectrum by using Eq. (7). Then the moving average of the current and voltage FFT spectrum is calculated. This moving average calculation is done by using Eq. (9) as follows,

$$\overline{MA} = \frac{1}{n} \sum_{i=1}^n D_i \quad (9)$$

where  $\overline{MA}$  is the moving average of data  $D$  every  $n$ -data points movement,  $D$  is the data which in this study is the current and voltage FFT data, and  $n$  is the length of the moving data that will be used for averaging. In this study, the current and voltage FFT moving average is calculated with 10 moving data points. This current and voltage FFT moving average will be used to subtract the current and voltage FFT data to obtain the zero mean average data. The zero mean average data helps to identify the presence of harmonics, fault, and significant peaks easier. By categorizing the peak as the outlier of these zero mean average data. The results of this identification process is the index locations of the peaks.

The identification of harmonics, fault, and significant peak indexes is done by using a moving windows. The moving windows size is half of the main frequency band. For example, with 60 Hz main frequency the moving windows size is 30 Hz band. So the peak identification is done in every 30 Hz from 0 Hz up to 13<sup>th</sup> harmonics which in this case is 780 Hz. After each searching on current and voltage frequency spectrum, the list of indexes found in both current and voltage spectrums will be combine by using union combination. These indexes will be used to find the magnitude and phase on the frequency spectrum of current per voltage data.

A bode plot of magnitude and phase will be generated through the identified frequencies in rad/s, magnitude in dB scale, and phase angle in degree. The bode plot is generated by frequency versus magnitude and by frequency versus phase angle. Generally, there will be two plots in bode diagram frequency versus magnitude plot and frequency versus phase angle. The bode diagram is plotted by using logarithmic scale for the frequency axis. A bode diagram represents a model of input-output relationship of a system. In our case, this bode diagram represents the relationship between input voltage and output current of the motor. So the pattern of the bode plot will define the complexity of the motor model. It is expected that this complexity of the motor model can be used to define the condition of the motor, either healthy or faulty. This method is essentially considered as the model-based fault diagnosis method as it considers the input and output relationship of the system.

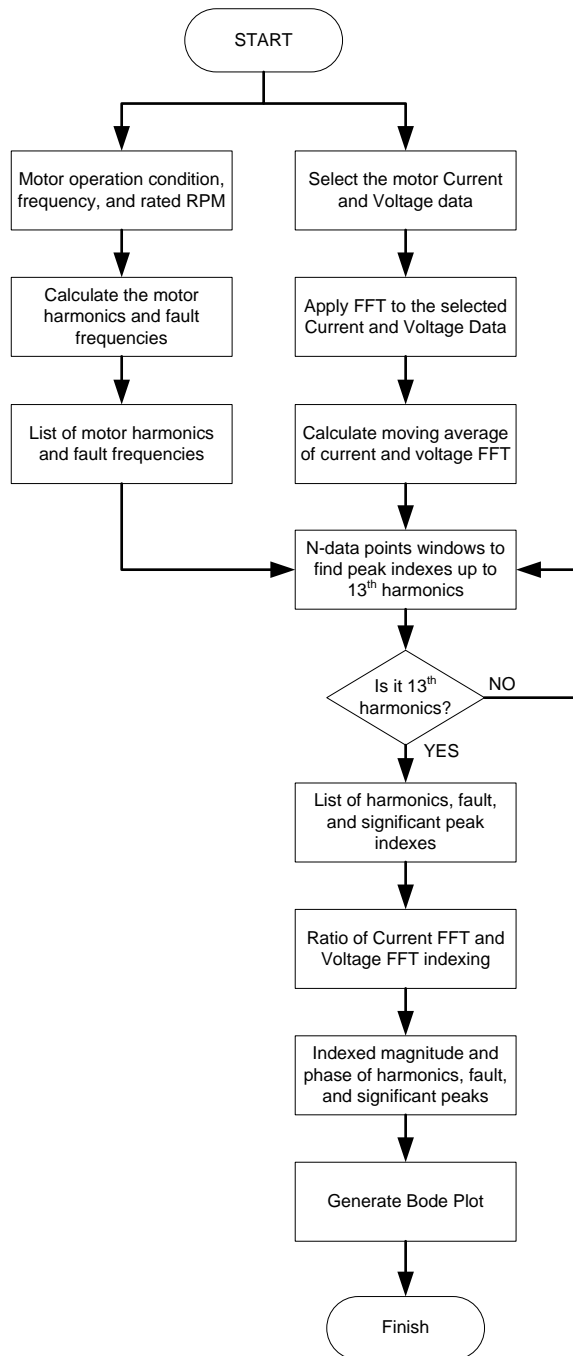


Fig. 3. Motor current per voltage bode diagram analysis

### EXPERIMENTAL RESULTS AND DISCUSSIONS

In this study, by using real induction motor parameter provided in (Duan and Živanović, 2014), the transfer function derivation of 3-phase induction motor model in ABC frame is done. It is found that for each phase output current there are three transfer function

contribution from the input voltage. An input voltage is given more weight on the contribution to the corresponding output current of the same phase compared to the other two-phase. For example, the input voltage phase-A is given more contribution for output current phase-A compared to the contribution for output current phase-B and phase-C. Therefore, the current per voltage analysis are focused on the same phase pair. Five operated induction motors are chosen as the examples. Three induction motors are operated under fault conditions, while the other two are operated under healthy conditions as shown in Table 1.

Motor 1 and 2 are operated at 60 Hz frequency at 3560 rated RPM and 1780 RPM. The results of MCSA of both motors can be seen in Fig. 4. Based on its current spectrum there is no fault frequency found. The Fig. 5 shows the bode diagram of current per voltage of both induction motor. Both motor use the pair of phase-A current and voltage for bode diagram analysis. This bode diagram will be our base comparison with the other motors with fault condition.

Two induction motors are operated under misalignment/unbalance fault conditions. Motor 3 is operated at 45.8 Hz frequency with 1750 rated RPM, while motor 4 is operated at 40 Hz frequency with 1750 rated RPM. Motor 3 uses the pair of phase-C current and voltage, while motor 4 uses the pair of phase-B current and voltage. Based on the Fig. 6, the current spectrum of both motor current signature shows two symmetrical side band peaks around the main frequency. By using Eq. (5) and (6) and the operating frequency, it can be calculated that the side band frequency of misalignment/unbalance fault is at 23.2 Hz and 68.6 Hz for motor 3 and is at 20.2 Hz and 59.8 Hz for motor 4 as shown in Fig. 6 and clearly observed. While from Fig. 7., the pattern of misalignment/unbalance fault can be seen from the current per voltage bode and phase diagram. Comparing to motor 1 and 2 shown in Fig. 5, a pattern can be found both in gain plot and phase plot and can be seen clearly in phase plot starting at  $\omega = 140 \text{ rad/s}$  and along both motor operating frequency to high order frequency. This frequency band is the location where normally misalignment frequencies are found. Therefore, the bode diagram at Fig. 7 shows that the misalignment motor models will have more zeros and poles on its transfer function compared to the bode diagram at Fig. 5.

Another induction motor sample is operated under bearing fault condition. The motor is operated at 53.2 Hz with 3555 rated RPM. Bearing fault frequencies can be calculated by using Eq. (1) to (4) with the bearing specification provided by the bearing manufacturer. It is then identified that the bearing failures is found. Fig. 8 (a) shows that there is no peak at bearing outer and ball frequencies, but there are peaks at bearing inner

Table 1. The observed industrial induction motor samples

Motor	Type	Frequency (Hz)	Rated Voltage (V)	Rated Current (A)	Rated RPM	Condition
Sample 1	Pump	60	460	214	3560	Healthy
Sample 2	Pump	60	480	66.3	1780	Healthy
Sample 3	Pump	45.8	380	55.7	1750	Misalignment/unbalance
Sample 4	Pump	40	380	55.7	1750	Misalignment/unbalance
Sample 5	Pump	53.2	480	130.74	3555	Bearing Faults

frequency at 313.36 Hz and bearing outer frequency at 215 Hz. Fig. 9 shows the drive end bearing inner ring, outer ring, and the bearing ball defects. This bearing inspection proves that the bearing defect signature observed at the current spectrum. The bode diagram shows different pattern of bearing fault compare to the misalignment/unbalance fault and healthy motor. As shown in Fig. 8 (b), motor sample 5 bode diagram with bearing fault shows a pattern at  $\omega = 15 \text{ rad/s}$  to  $\omega = 165 \text{ rad/s}$ .

Bode diagram pattern represents the input-output relationship of the system as it is generated from the input and output of the system. As it can be seen from Fig. 5, Fig. 7, and Fig 8 (b), different condition of the induction motor shows different pattern of bode diagram. It reflects that the healthy motor model structure will be

simpler than the faulty model structure. The bode diagram pattern of the faulty motors show more zeros and poles in their model structure. The difference in complexity of the healthy and faulty motors will generate different outputs in which the residual of these outputs can be compared to determine the fault type and level of the motor condition. In this study 3-phase voltage and 3-phase current are employed in order to do the current per voltage bode diagram based FDD. There are 9 bode diagrams of each motor, but it is chosen only 1 bode diagram that shows severity in their model structure to be presented in this paper. These pattern can actually also be seen in the other bode diagrams but in different magnification.

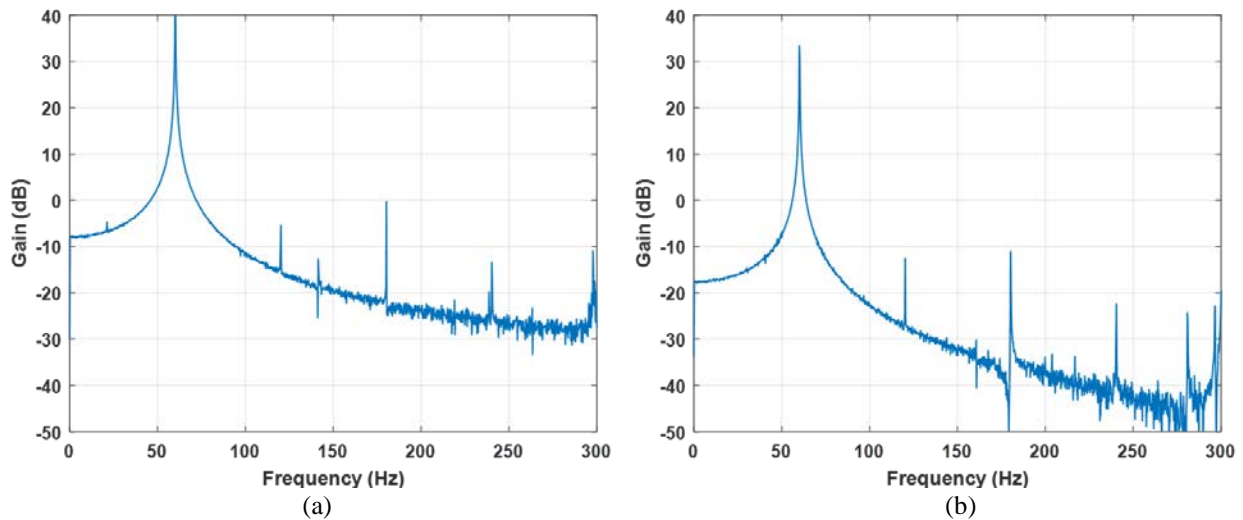


Fig. 4. Healthy motor current frequency spectrum plots (a) motor sample 1, (b) motor sample 2

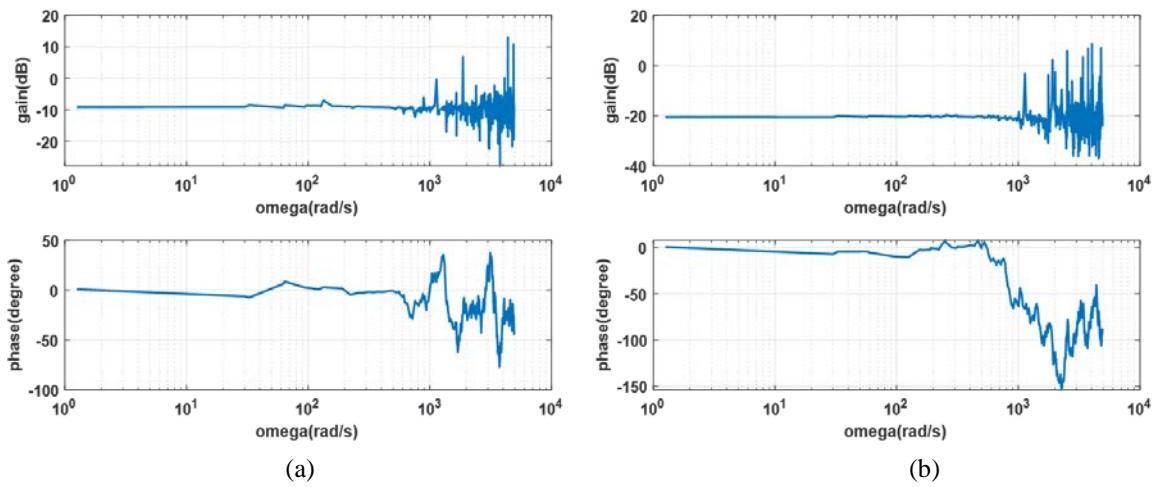


Fig. 5. Healthy motor magnitude and phase logarithmic plots (a) motor sample 1, (b) motor sample 2

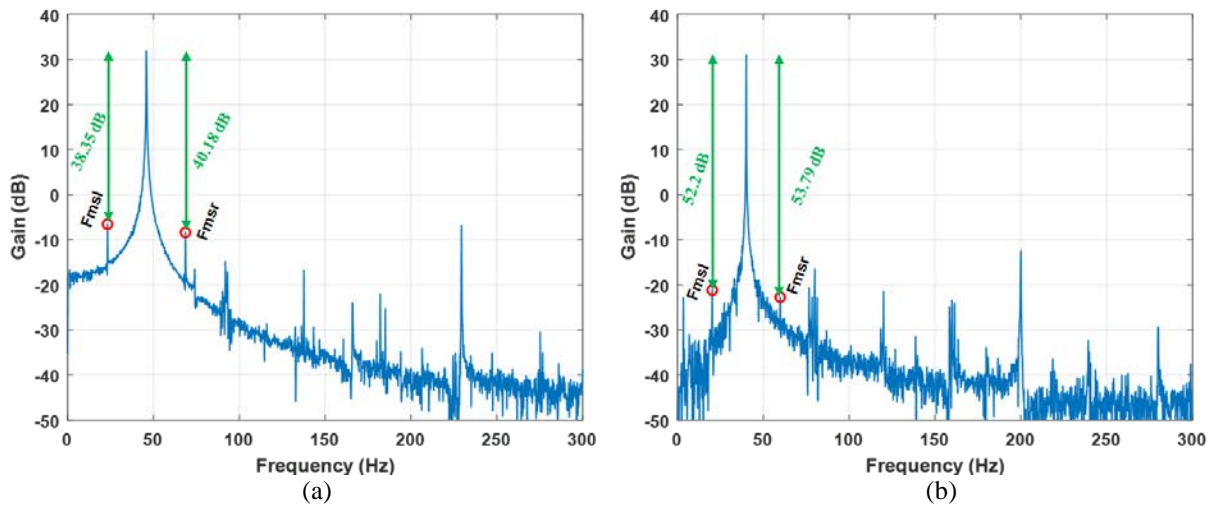


Fig. 6. Misalignment/unbalance fault motor current frequency spectrum plots (a) motor sample 3, (b) motor sample 4

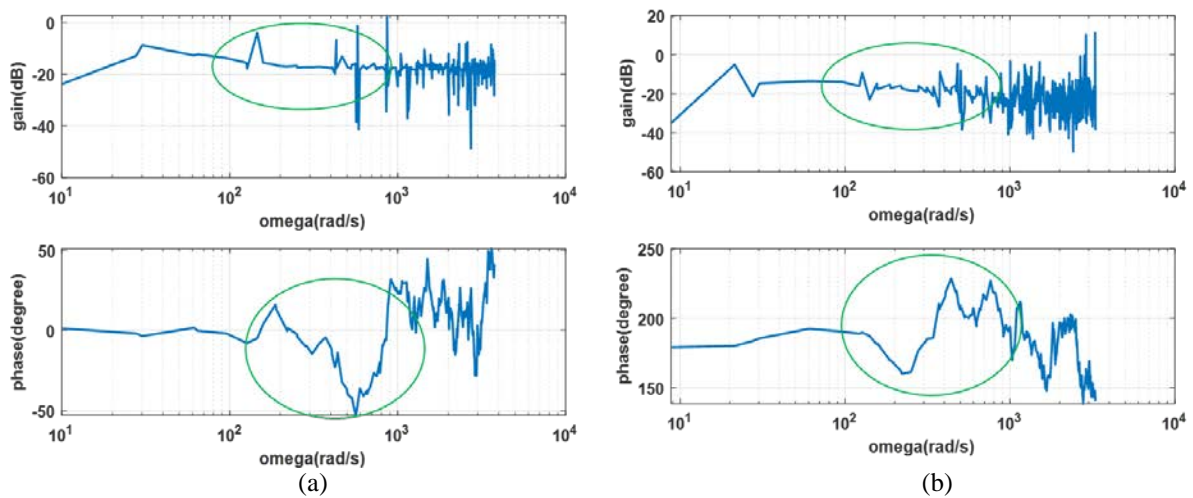


Fig. 7. Misalignment/unbalance fault motor magnitude and phase logarithmic plots (a) motor sample 3, (b) motor sample 4

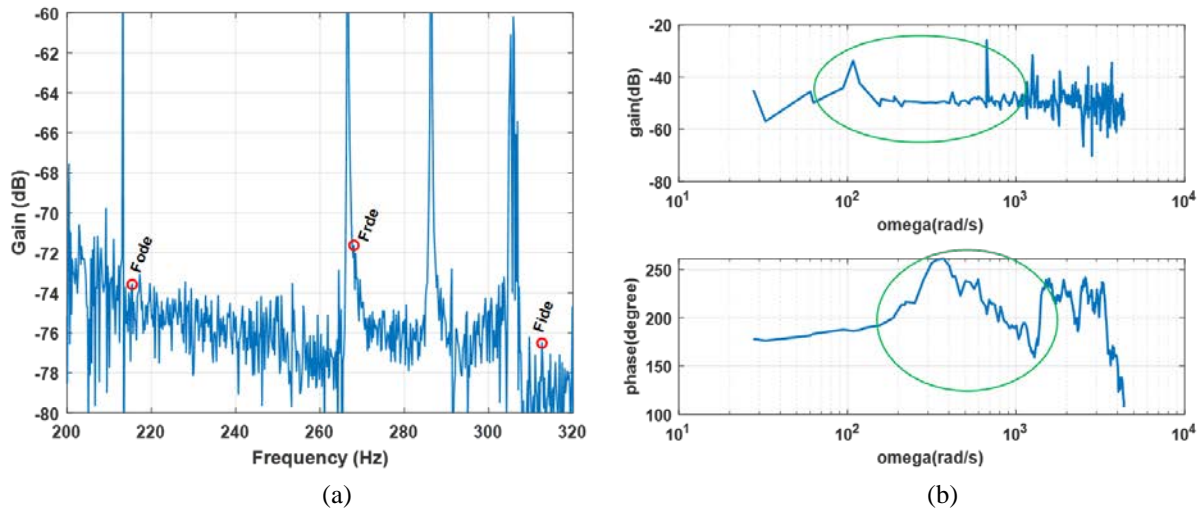


Fig. 8. Bearing fault motor sample 5 (a) current frequency spectrum, (b) magnitude and phase logarithmic plots



Fig. 9. Motor sample 5 drive-end bearing defects (a) bearing inner and outer ring, (b) ball bearing

## CONCLUSIONS

A novel fault detection and diagnosis method is proposed in this study by considering motor harmonics, fault, and significant peak frequencies on the current per voltage frequency spectrum. The fault detection and diagnosis is performed by observing the pattern of the current per voltage bode diagram. This method is compared with the existing motor current signature analysis. The MCSA successfully identify the presence of fault frequencies in the current frequency spectrum in the example cases, while the current per voltage bode diagram observation also detect and distinguish different motor conditions. Healthy motor pattern in bode diagram is simpler compared to faulty motor. In addition, between misalignment/unbalance fault and bearing fault condition it shows different bode diagram pattern implying that different fault generates different model structure.

This finding is important in preliminary understanding of the difference between healthy and

faulty motor model structures. With different model structure, the simulated current output from healthy and faulty motors will be different. The pattern and the residual between their outputs can be used to detect and classify the fault type and define the level of fault severity. This comparison between the healthy and faulty motor model structure output will be the future work of this study.

## ACKNOWLEDGEMENT

This research was sponsored by the Ministry of Science and Technology, Taiwan, R.O.C. under Grant No. MOST 108-2218-E-011-020-. Part of the funding also came from the Industry-University Cooperated Project with Innolux Corporation.

## REFERENCES

Duan, F. and Živanović, R. 'Condition monitoring of an induction motor stator windings via global

- optimization based on the hyperbolic cross points', *IEEE Trans. Ind. Elec.* IEEE, Vol. 62, No. 3, pp. 1826–1834. (2014).
- Guo, H. and Liu, M.-K. 'Induction motor faults diagnosis using support vector machine to the motor current signature', in *2018 IEEE Industrial Cyber-Physical Systems (ICPS)*. IEEE, pp. 417–421. (2018).
- Hsu, W.-T. *et al.* 'Fault Signature Analysis of Industrial Machines', in *IFTOMM International Symposium on Robotics and Mechatronics*. Springer, pp. 346–359. (2019).
- ISO 10816-3 Mechanical vibration evaluation of machine vibration by measurements on non-rotating Parts* (1998).
- ISO 20958 Condition monitoring and diagnostics of machine systems - Electrical signature analysis of three-phase induction motors* (2013).
- Jung, J.-H., Lee, J.-J. and Kwon, B.-H. 'Online diagnosis of induction motors using MCSA', *IEEE Trans. Ind. Elec.* IEEE, Vol. 53, No. 6, pp. 1842–1852. (2006).
- Jung, J. *et al.* 'Electrical monitoring of mechanical looseness for induction motors with sleeve bearings', *IEEE Trans. Energy Convers.* IEEE, Vol. 31, No. 4, pp. 1377–1386. (2016).
- Liu, M.-K. and Weng, P.-Y. 'Fault Diagnosis of Ball Bearing Elements: A Generic Procedure based on Time-Frequency Analysis', *Meas. Sci. Rev. Sciendo*, Vol. 19, No. 4, pp. 185–194. (2019).
- Mitra, S. K. and Kuo, Y. *Digital signal processing: a computer-based approach*. McGraw-Hill New York. (2006).
- Nandi, S. *et al.* 'Detection of eccentricity faults in induction machines based on nameplate parameters', *IEEE Trans. Ind. Elec.* IEEE, Vol. 58, No. 5, pp. 1673–1683. (2010).
- Nandi, S., Toliyat, H. A. and Li, X. 'Condition monitoring and fault diagnosis of electrical motors—A review', *IEEE Trans. Energy Convers.* IEEE, Vol. 20, No. 4, pp. 719–729. (2005)
- Ortiz, A. *et al.* 'Detection of misalignment in motor via transient current signature analysis', in *2019 IEEE International Conference on Engineering Veracruz (ICEV)*. IEEE, pp. 1–5. (2019).
- Popaleny, P. and Antonino-Daviu, J. 'Electric Motors Condition Monitoring Using Currents and Vibrations Analyses', in *2018 XIII International Conference on Electrical Machines (ICEM)*. IEEE, pp. 1834–1840. (2018).
- Schoen, R. R. *et al.* 'Motor bearing damage detection using stator current monitoring', *IEEE Trans. Ind. App.* IEEE, Vol. 31, No. 6, pp. 1274–1279. (1995).
- Sullivan, G. *et al.* *Operations & maintenance best practices-a guide to achieving operational efficiency (release 3)*. Pacific Northwest National Lab.(PNNL), Richland, WA (United States). (2010).
- Thomson, W. T. and Culbert, I. *Current signature analysis for condition monitoring of cage induction motors: industrial application and case histories*. John Wiley & Sons. (2017).
- Wang, J. *et al.* 'Multilevel Information Fusion for Induction Motor Fault Diagnosis', *IEEE/ASME Trans. Mechatronics*. IEEE, Vol. 24, No. 5, pp. 2139–2150. (2019).
- Yang, T. *et al.* 'Feature knowledge based fault detection of induction motors through the analysis of stator current data', *IEEE Trans. Instrum. Meas.* IEEE, Vol. 65, No. 3, pp. 549–558. (2016).

## 使用電壓電流波德圖之感應馬達異常診斷的新穎方法

Widagdo Purbowaskito 藍振洋 劉孟昆  
國立台灣科技大學機械工程學系

### 摘要

本研究旨在探討感應馬達之異常偵測與診斷，相較於傳統的振動頻譜分析方法或電流特徵頻譜分析方法，文中提出以馬達電壓電流所產生之波德圖來判斷感應馬達之狀態。將感應馬達轉動設備視為一個系統，其電壓為系統之輸入，電流為系統之輸出。藉由產生之感應馬達電壓電流波德圖的樣式模型，用來判斷馬達之狀態。波德圖主要描述一系統的輸入輸出之關係。因此本方法也可視為模型式之異常偵檢方法，期改善電流特徵頻譜分析中電壓雜訊之干擾。先期應用於五組感應馬達設備，其中兩組為健康設備，兩組為具有不平衡/不對心之異常設備，一組為有軸承異常之設備。其結果顯示不同狀態的馬達顯示出明顯不同之波德圖的樣式模型。